N. Zhu, X. Huang, J. Fang, L. Yang, L. Hu (2020) *Transitional flame-spread and fuel-regression behaviors under the change of concurrent wind,* **Fire Safety Journal** – Special Issue of IAFSS International Symposium. https://doi.org/10.1016/j.firesaf.2020.103015

Transitional flame-spread and fuel-regression behaviors under the change of concurrent wind

Nan Zhu[a], Xinyan Huang[b,*], Jun Fang[a], Lizhong Yang[a], Longhua Hu[a,*]

[a] *State Key Laboratory of Fire Science, University of Science and Technology of China, Hefei, Anhui, 230026, PR China*

[b] *Department of Building Service Engineering, Hong Kong Polytechnic University, Kowloon, Hong Kong, China*

*Corresponding author: xy.huang@polyu.edu.hk; hlh@ustc.edu.cn

Highlights:

- A transition flame spread process was found from still air to concurrent flow
- The transition of flame spread rate and the fuel-rear regression rate was quantified.
- Wind effect on flame spread and fuel regression was analysed separetly.

Abstract:

On the occurrence of an environmental wind, the steady-state flame spread will go through a transitional process to a new steady state of the concurrent flame spread. However, such a transition between two steady states was rarely studied, despite that it often happens to many fire events. This paper presents an experimental study on the transitional flame-spread behavior over the horizontal PMMA plate by applying different concurrent airflows from the still air. The flame spread rate at the pyrolysis leading edge and the regression rate in the fuel rear end were studied during this transition region. It was found that the transition stage could be divided into three regions based on both the length of pyrolysis and the fuel regression rate, (1) increasing to maximum, (2) dropping from peak, and (3) reaching the new steady-state value. The wind velocity is found to have different influence on the flame spread rate and fuel-rear regression rate during the transition. This work provides novel experimental data on the transitional behavior of flame spread under the change of concurrent wind, which helps evaluate the fire hazard under the sudden change of environmental conditions.

Keywords: Fire spread, Concurrent wind, Wind change, Flame spread rate, Regression rate, Pyrolysis length.

Nomenclature

L_p	pyrolysis length (cm)	***Greek symbols***	
L_f	flame length (cm)	ρ	density (kg/m^2)
$\dot{m}''$	fuel regression rate (g/m^{2}s)	θ	flame tilt angle from vertical (degree)
$\dot{q}''$	heat flux (W/m^2)	***Subscripts***	
t	time (s)	f	flame
T	temperature (K)	g	gas
u_∞	wind velocity (m/s)	r	radiation
v_f	flame spread rate (cm/min)	rr	reradiation
δ_f	preheating length (cm)	s	solid
$Y_{O_2,\infty}$	environmental oxygen concentration	$loss$	heat loss
h_f	flame height (cm)	∞	ernvironment
L_v	effective heat of vaporization (J/kg)		

1. Introduction

Flame spread over solid combustible under wind conditions has received more attentions in recent years, due to the complex heat transfer mechanism in gas-solid phase and increasing number of fire events in the building facade and wildland. Such flame spread behavior could be divided as opposed- or concurrent motions, based on the direction of the air flow relative to that of the flame propagation over the fuel surface. Opposed flame spread, i.e., the direction of the air flow is opposite to that of the flame propagation, has been studied and reviewed in [1-4]. The opposed flame spread is controlled by the convection heat transfer in the forced convection boundary layer at the flame leading edge. The characteristic preheating length and the boundary layer thickness, which together control the convection heat transfer, could be well resolved based on the boundary layer solution theory. In contrast, the concurrent flame spread, that the direction of the air flow is same as the flame propagation, is much more complicated due to the turbulent flame boundary layer and the complex interaction between flame and fuel. Thus, research on concurrent flame spread is still relative limited, compared with the opposed flame spread.

The reported studies on concurrent flame spread behavior focused on the steady-state condition, i.e., the measurement was taken when the flame spread rate (FSR) or mass burning rate remained constant [5-13]. Loh and Fernandez-Pello [10] studied flame spread in concurrent forced flow and found a linear relationship between FSR (v_f) and air flow velocity (u_∞): $v_f \sim u_\infty Y_{O_2,\infty}^2$, where $Y_{O_2,\infty}$ is oxygen concentration in the air flow. Hu [14-18] investigated the evolution of flame shape, fuel burning rate and flame heat flux feedback in cross air flow, the relative importance of different

heat feedback mechanism was found to be altered prominently due to the deflection of the flame. Quintiere [19] proposed following qualitative relation between FSR and heat flux in preheating zone ($\dot{q}_f^{"}$):

$$v_f = \frac{4\left(\dot{q}_f^{"}\right)^2 \delta_f}{\pi\left(k\rho c_p\right)\left(T_p - T_\infty\right)^2} \tag{1}$$

where δ_f is the preheating length between flame tip and pyrolysis front. According to Eq. (1), FSR is influenced by flame heat flux $\dot{q}_f^{"}$ which is significantly different in concurrent flow comparing to that in still air. Tang et al. [20] studied heat flux distribution under concurrent forced flow, which showed to decrease exponentially with downstream distance. Ju et al. [21] studied heat flux in preheating region and modified radiation and convection heat flux with flame thickness. Singh and Gollner [7] studied heat flux distributions in burning region, where convection, radiation heat flux were measured by experimental methods. Radiation heat flux was measured to be only 19.61% of total incident heat flux for concurrent cross airflow velocity of 2.06 m/s, which is much lower than 80% in still air shown in Jiang's work [22]. It can be seen that relative importance of radiation in flame spread decreases obviously as the increased concurrent airflow enhanced the convective heating.

One should note that, for the concurrent flame spread, there is a considerable transitional acceleration stage before reaching the steady state, especially for over the thick fuel. Comparatively, the transitional stage in the opposed flame spread is much shorter. However, research on this transitional stage is still very limited. Zhao et al. [23] observed an increasing flame length transitional stage after the fuel was ignited from his experiments on flame spread under concurrent forced flow on a thin composite cotton-fiberglass fabric blend. The transition state was defined before flame length kept constant with time. Tseng and Tien [24] studied flame growth of thin solid fuel using computational models. The transition state and steady state could be distinguished by pyrolysis length. Apte et al. [25] studied this transition stage using large PMMA samples. It was found that flame height, flame length and flame spread rate changed with time obviously. Based on the different flame shape, flame spread process was divided into two modes: boundary mode and plume mode. Mass burning rate kept constant in boundary mode and increased as fire propagates in plume mode.

Moreover, when an airflow is suddenly imposed, the original steady-state flame spread in the still air will accelerate and transition to a new steady state. Such fire behavior happens more often in real fire scenarios, which is more realistic compared to the idealized steady-state flame spread under the still air condition or the concurrent airflow. It could be anticipated that the transition of pyrolysis front and fuel rear end could behave differently before they finally reach the new steady state. However, there is still no work reported on the transition behavior of flame spread on above basic scenario.

In the present study, experiments were conducted to study the transition of flame spread over PMMA surface from condition in still air to that with a concurrent forced airflow imposed. The evolutions of the pyrolysis front (representing flame spread) and fuel rear end (representing fuel-regression), as well as the pyrolysis length were quantified. Influence of wind on the flame spread rate and regression rate was also discussed.

2. Experimental approach

2.1 Experimental setup

Figure 1 shows experimental setup where the forced air flow was produced by a wind tunnel with a cross sectional size of 1.5 m width and 1.3 m height. The total length of the tunnel was 72 m. Experimental rig was positioned outside and close to outlet portal with a distance of 0.4 m. The air flow velocity remained constant from inside the tunnel to the experimental apparatus, which was monitored by a 4-probe hot-wire anemometers (accuracy: 0.01 m/s). During the experiments, a reasonably uniform horizontal wind was blown along sample sheets (uniformity > 95%). Six air flow conditions were conducted for studying the flame spread characteristics: 0 (quiescent), 0.3, 0.6, 0.9, 1.2 and 1.5 m/s.

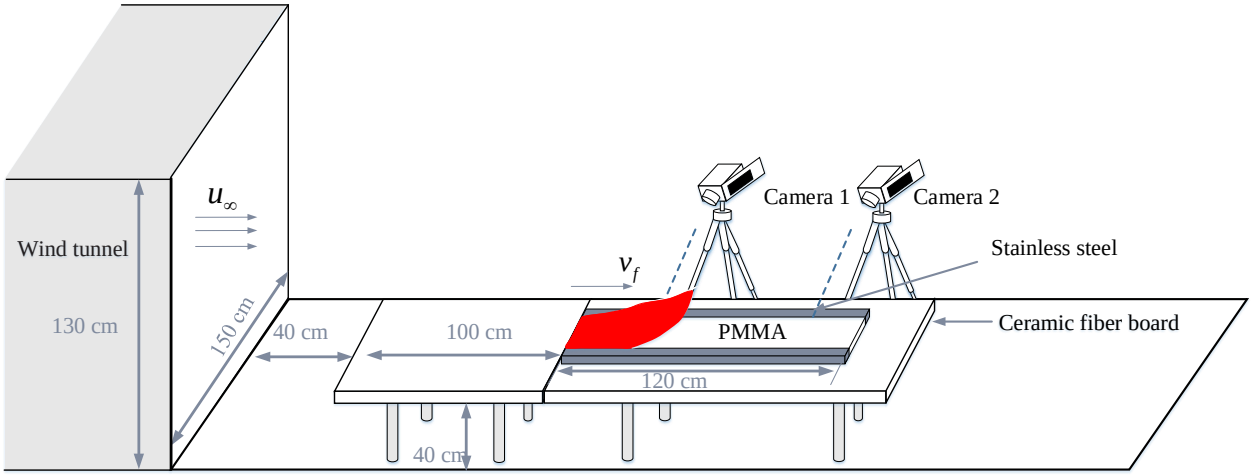

Fig. 1 Experimental setup.

Flat PMMA sheets of 4 mm thickness were selected as the representative non-charring fuel. The length of the sample was 120 cm and the width was 10 cm. During the experiments, PMMA samples were placed on a 2.5-cm-thick ceramic fiber board for thermal insulation. The ceramic fiber board was 1 m wide and the sample sheet was placed in the middle of the board. Before the sample sheet, a 1-meter-long ceramic fiber board was used to smooth the air flow. The PMMA sample was sandwiched between stainless steels on both sides perpendicular to the flow, only the upper surface of the sample was allowed to burn.

Ignition was achieved by a strip of ethanol-soaked filter paper. After ignition, the flame was allowed to spread in still air for 16.67 min (or 1000 seconds) to reach steady flame spread rate.

Then flame spread rate and pyrolysis length kept constant and the influence of ignition source could be ignored [26]. After that the forced air flow was introduced by starting the wind tunnel. The flame spread transits from that of a steady state in still air to that in a concurrent air flow, accelerating and finally reaches another steady state. The overall test time was around 40 min to 80 min depending on the wind speed (time is less as the wind speed is higher) to ensure that it reaches the steady state after concurrent air flow was imposed.

2.2 Measurements

The process of flame spread as well as flame shape were recorded by two digital video cameras with resolution of 1920×1080 and film speed of 25 fps, providing side-view images of burning region. From these images the positions of pyrolysis front and fuel rear end during flame spread process could be identified. As burning region is short compared with the length of sample sheets, the camera was set with a relative narrow view scope for explicit images. Two cameras were placed side by side to record half of the sample sheets, respectively, which together provides the whole record of the flame spread process over the sample.

The positions of the pyrolysis front and fuel rear end were recorded by images of camera 1 and camera 2 at 1 min interval. The pyrolysis length could be deduced as the difference of the pyrolysis front and pyrolysis rear. FSR was determined as the moving speed of pyrolysis front, which is calculated as the derivative of pyrolysis front positions with respect to time. All experiments were conducted twice and the averaged results were taken from the experiments.

Figure 2 shows flame condition and characteristic lengths in concurrent flow during the spread. The flame is blown towards the fuel, which leads to a larger flame heat flux $\dot{q}_f^{''}$ to the fuel. So that the flame spread rate is larger than that of still air. Preheating length is the horizontal distance between flame tip and pyrolysis front, which influences the flame heat flux to the unburned fuel and flame spread rate. Pyrolysis length is defined as horizontal distance between pyrolysis front and pyrolysis rear, which influences amount of combustible gas and flame length.

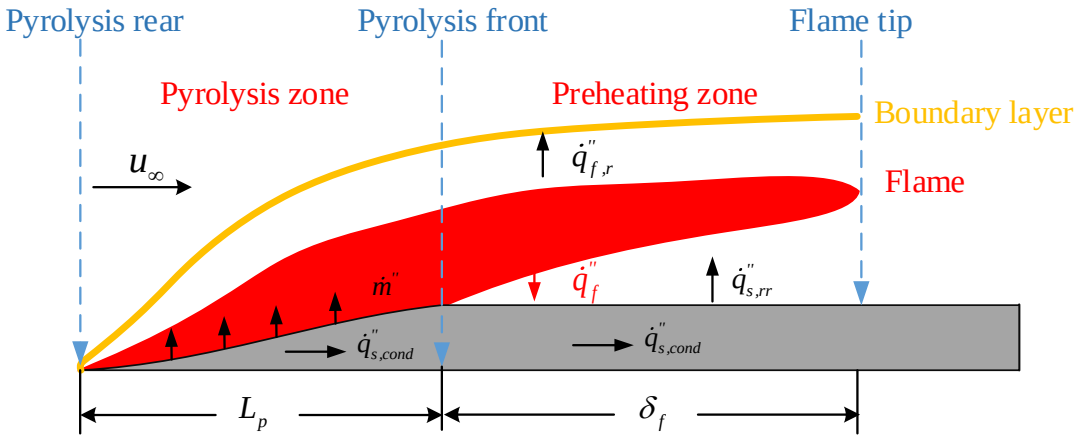

Fig. 2 Definition of flame characteristic lengths.

3. Results and discussion

3.1 Pyrolysis length

Figure 3 shows typical images of burning region during flame spread process. The velocity of wind u_∞ is 0.9 m/s. Burning region is bright in the images. The shape of pyrolysis front and fuel rear end is curved. The pyrolysis front and fuel rear end are defined as the tip of the curve. It can be seen from the images, pyrolysis length L_p increases from 0 min to 16 min, and decreases from 16 min to 24 min. After 24 min, L_p keeps constant along flame spread process, which is not presented in detail here. From the images a transition state can be found between steady state in still air and that in concurrent air flow.

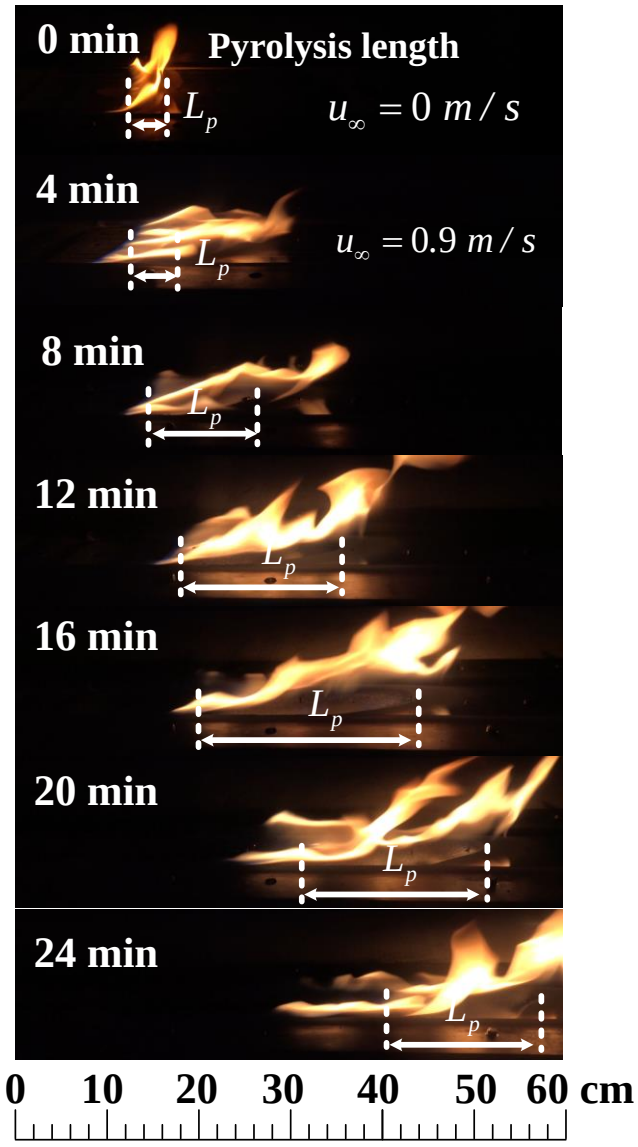

Fig. 3 Typical images of burning region of PMMA sheets (wind velocity is 0.9 m/s, wind is employed since 4 min in the figure).

Figure 4 shows the spreading distance of pyrolysis front and fuel rear end with time, with the air flow velocity of 0.9 m/s. The change of burning region in the other experiment conditions are of the similar trend with Fig. 4. The spreading process of pyrolysis front can be divided into three Regions:

I. (< 16 min) flame spread in steady state in still air. The flame spread rate, which can be calculated as the slope of spreading distance of pyrolysis front, is rather slow;

II. (16 – 28 min) after the concurrent air flow is imposed, the flame spread rate turns to be faster than still air. This increase happens within one minute after the air flow increases from the still air, as flame shape changes immediately in concurrent flow;

III. (> 28 min) the flame spread slows down and reaches a new steady state.

The observed flame spreading in pyrolysis rear is essentially the regression rate. In Region I, fuel-rear regression rate is the same as flame spread rate in still air. In Region II and III, the fuel-rear regression rate accelerates gradually and reaches the peak. Afterwards, in Region IV, the fuel-rear regression rate turns to be smaller than before, then it keeps uniform and the same as pyrolysis front when the steady state in concurrent air flow is reached. Pyrolysis length L_p is determined by flame spread rate and fuel-rear regression rate. The relative uncertainty of the measured pyrolysis length is estimated to be less than 10.16% with 95% confidence. The average values are used for further analysis.

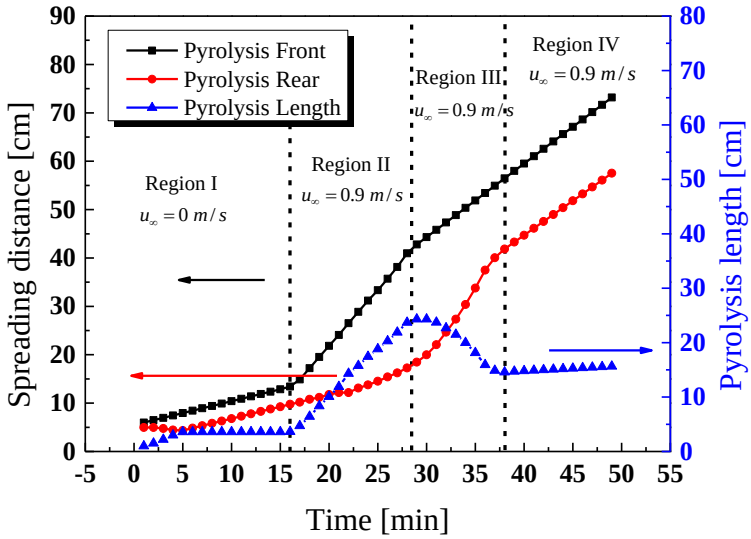

Fig. 4 Pyrolysis front, fuel rear end, and pyrolysis length over time. (u_∞ =0.9 m/s).

According to the evolution of pyrolysis length, the flame spread process in Fig. 4 can be divided into four regions. In Region I, L_p keeps uniform with time. In region II, L_p increases with time and reaches the peak at the end of the region, as flame spread rate is larger than fuel-rear regression rate. In region III, L_p decreases gradually with time, which means the fuel-rear regression rate in this period is larger than flame spread rate. At the end of region III, L_p reaches the nadir. Then L_p

keeps constant in Region IV, where the flame spread rate and the fuel-rear regression rate are the same.

In Fig. 4, Region I represents the steady state in still air. After the air flow is employed, both the flame spread rate and fuel-rear regression rate changes from Region I, and a transition flame spread state is reached in Region II and Region III. In Region III, the flame spread rate is unchanged, while fuel-rear regression rate increases with time. In Region IV, the flame spreads in steady state and L_p remains constant with time.

3.2 Flame spread rate

Figure 5 plots the time evolution of flame spread rate during the transitional state. It can be seen that for all wind conditions, similar evolution can be observed on flame spread rate. The flame spread rate is slow in still air. After the wind is applied, the flame spread rate increases rapidly. This is due to the distinctive change of flame condition, hence heat feedback to fuel surface, in concurrent flow relative to that in still air. The flame spread rate is mainly influenced by the flame heat flux $\dot{q}_f^{''}$ and the heating length (δ_f) to unburned fuel. In concurrent flow, flame is blown towards unburned fuel, leading to greater flame heat flux and effective heating length. Thus, an immediately increase of flame spread is expected, right after the air flow is employed.

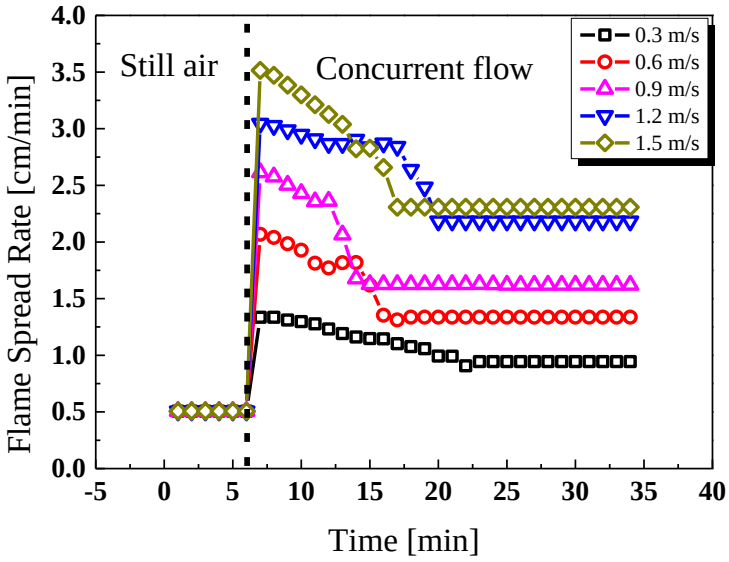

Fig. 5 Transient flame spread rate.

As flame spreads in concurrent flow, pyrolysis length increases gradually, which leads to an increase in both the flame size and the strength of buoyancy compared with forced flow. Consequently, the flame gradually "stands up" and flame heat flux to unburned fuel $\dot{q}_f^{''}$ decreases, which is defined as the transition from "plume mode" to "boundary layer mode" in [20]. As a result, the flame spread rate decreases gradually in concurrent flow. Afterwards, the flame spread rate reaches a new steady state. As the wind speed increases, the flame spread rate increases because the wind pushes the flame closer to unburned fuel.

Figure 6 further compares the steady flame spread rate with previous experiments of Loh et al. [10] with 10-cm wide and 12.7-mm thick PMMA samples, and Huang and Gollner [27] with inclined thick PMMA plates. The equivalent wind velocity of buoyancy entrainment can be calculated based on flame tilt angle and flame height

$$u_\infty = cos(\theta)\sqrt{gh_f} \tag{2}$$

where θ represents flame tilt angle from vertical, h_f represents flame height. From Fig. 6, a linear relationship can be seen between steady spreading rate and the concurrent wind velocity [10].

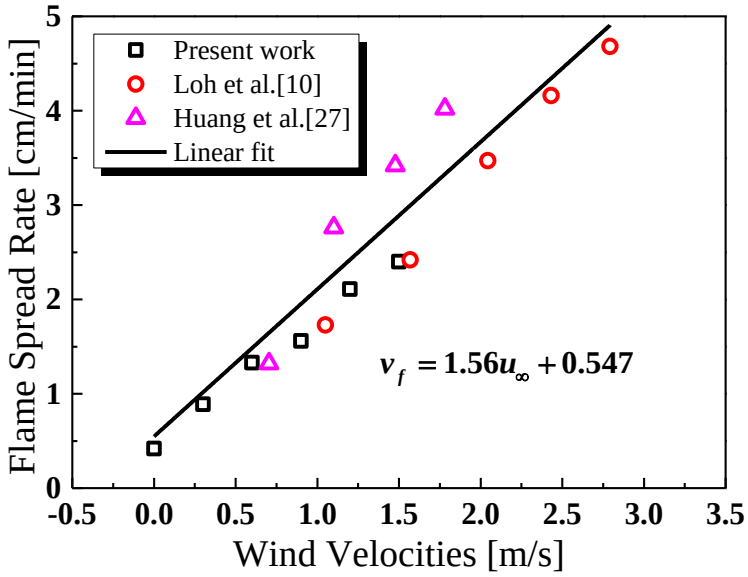

Fig. 6 Steady flame spread rate. Here steady spreading rate is compared with previous experimental results by Loh et al. [10] and Huang and Gollner [27] where sample width is 10 cm and sample thickness is 12.7 mm.

3.3 Fuel-rear regression rate

Figure 7 shows the evolution of fuel-rear regression rate, which is quite different from the pyrolysis front. It can be observed that the fuel-rear regression rate increases with wind velocities. When the wind is blown to the solid fuel, fuel-rear regression rate gradually changes from still air to concurrent flame spread state. For an imposed wind velocity, fuel-rear regression rate first increases with time, and reaches the peak. Then, it decreases until a constant value. The steady-state fuel-rear regression rate is the same as flame spread rate in Fig. 5. In other words, the overall fuel burning rate also reaches the steady state.

It can be found that the change in fuel-rear regression rate is different from flame spread rate, which shows different "sensibility" of pyrolysis front and fuel rear end to wind speeds. As shown in Fig. 8, for pyrolysis front, flame spread rate is influenced by flame heat flux $\dot{q}_f''$ to unburned fuel, which is essentially influenced by flame tilt angle.

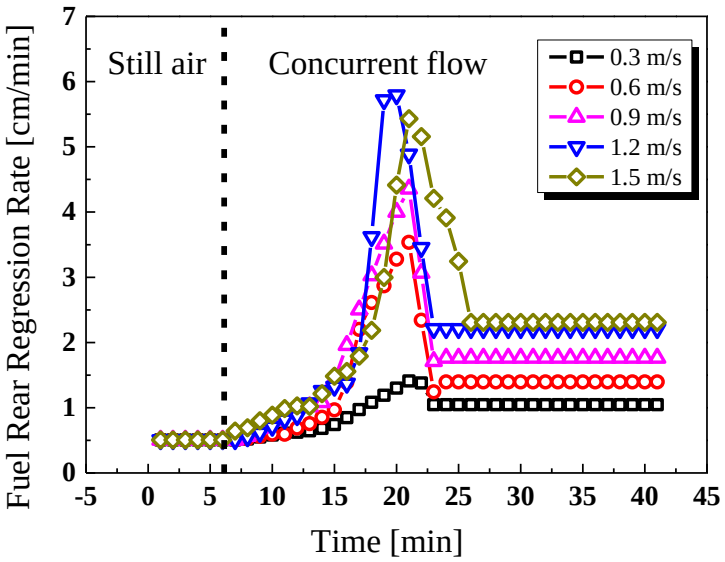

Fig. 7 Transient fuel-rear regression rate.

For pyrolysis rear, the spreading rate is actually the fuel regression rate. And fuel rear end moves with the burn-out or regression of fuel, which is controlled by flame heat flux to pyrolysis fuel [26, 28]. The burning rate of pyrolysis fuel $\dot{m}''$ was found to be controlled by convection heat flux in concurrent flow, which is estimated by boundary layer thickness in burning region [7]. It was found that boundary layer thickness decreases with wind velocities and convection heat flux $\dot{q}''_{f,c}$ increases [8]. The energy balance of fuel regression rate at fuel rear end is:

$$\dot{m}'' L_v = \dot{q}''_{f,c} + \dot{q}''_{f,r} - \dot{q}''_{s,cond} - \dot{q}''_{loss} \tag{3}$$

where $\dot{q}''_{f,c} + \dot{q}''_{f,r}$ represents flame heat flux to pyrolysis rear, $\dot{q}''_{s,cond}$ represents heat transfer through solid phase, $\dot{q}''_{loss}$ is the heat loss through gas phase. The increase of convection heat flux $\dot{q}''_{f,c}$ leads to the increase of fuel-rear regression rate with wind velocities. Wind effect also causes the local blow-off phenomenon at pyrolysis rear, which increases the $\dot{q}''_{loss}$ and decreases the burning rate of the fuel at pyrolysis rear. However, this heat loss is relatively small compared with the increases of heat flux in low wind velocities. So that the fuel-rear regression rate increases with wind speed in this experiment. However, the influence of local blow-off phenomenon increases with wind velocities. At high wind velocity conditions, the heat loss $\dot{q}''_{loss}$ at fuel rear end cannot be neglected, which can be seen from Fig. 7 that the difference of fuel-rear regression rate between wind velocity of 1.2 m/s and 1.5 m/s is rather small.

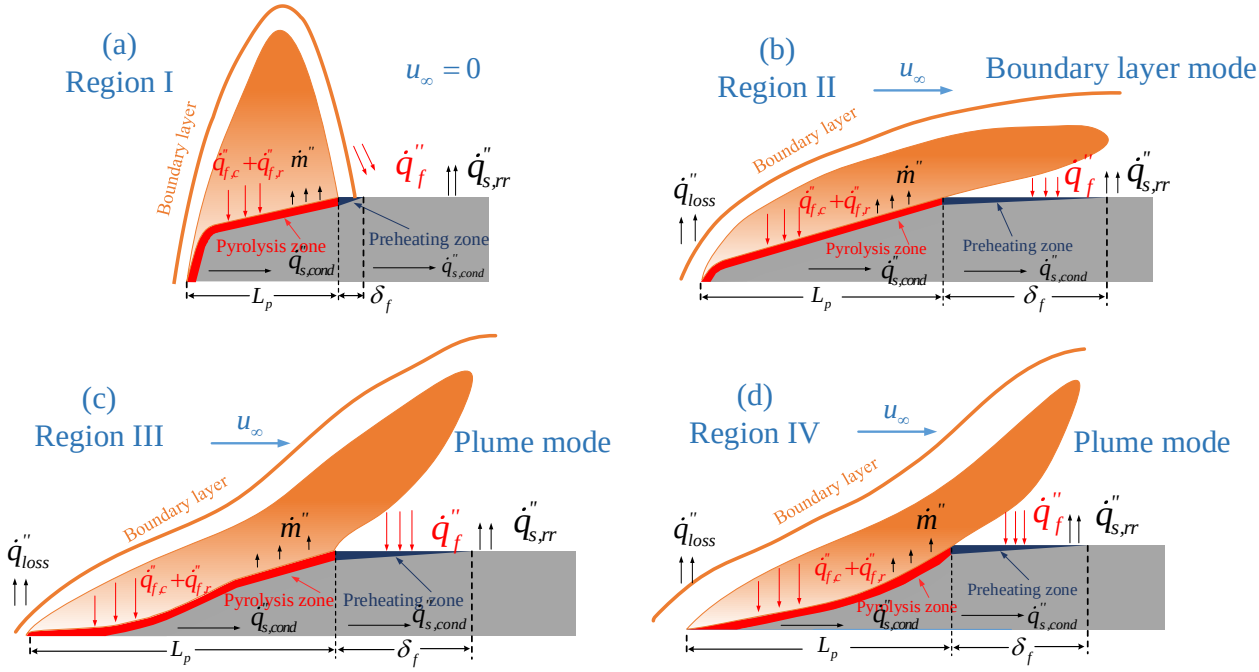

Fig. 8 Schematic diagram of burning region (a): Region I in still air (b): Region II in concurrent flow (c): Region III in concurrent flow (d): Region IV in concurrent flow.

Because of the larger regression rate at the fuel rear end under the concurrent flow, the thickness of fuel rear end decreases during the transition process in concurrent flow and leads to an accelerating fuel-rear regression rate of the fuel. Figure 8 also illustrates the deformation process of the pyrolysis rear end. Fig. 8(a) shows the steady flame spread state in still air. After the air flow is employed, thickness of boundary layer at fuel rear end decreases, which increases the convection heat flux $\dot{q}''_{f,c}$ to pyrolysis rear. So that the fuel regression rate is larger than in still air and thickness of fuel rear end decreases gradually during transition process in concurrent flow, as it can be seen from Fig. 8(b) to Fig. 8(d). The evolution of fuel-rear regression rate, or namely its response to air flow opposed, is influenced by fuel thickness and pyrolysis length, which changes during transition state. Such transition for fuel-rear regression rate takes relatively longer time compared with that of flame spread rate (Fig. 4).The fuel-rear regression rate reaches the peak where thickness of fuel rear end is rather small. After that, it decreases to steady value and transition flame spread state turns to be steady state.

4. Conclusions

Experimental investigation was conducted on PMMA sheets with different flow velocities, to reveal the transitional flame-spread and fuel-regression behaviors under the change of concurrent wind from that in still air. The flame spread rate, fuel-rear regression rate, as well as pyrolysis length were measured to quantify the transitional flame spread process. Major findings can be drawn as following:

(1) A transition flame spread state was found in concurrent flame spread process. During the transition state, pyrolysis length first increased from that of still air, and then decreased to steady value. The evolution of pyrolysis length was due to the difference between flame spread rate and fuel-rear regression rate, which shows different influence of wind on different pyrolysis regions.

(2) In transition flame spread process, flame spread rate first increased rapidly from still air because of the increasing flame heat flux to unburned fuel, and then decreased to steady value gradually due to the increase of buoyancy strength compared with forced flow. Steady flame spread rate increased linearly with wind velocities.

(3) The fuel-rear regression rate increased with wind velocities because of the increase of flame heat flux to the burning region. During transition flame spread process in concurrent flow, fuel-rear regression rate first increased gradually from that of still air because of large flame heat flux and the decrease of fuel thickness of pyrolysis rear, then decreased to steady value.

The present study provides for the first time the experimental data and quantification of this transitional behavior of flame spread under the change of concurrent wind. The sample width effect and thickness effect could have essential contribute to the transition process in concurrent air flow, which will be studied in the future.

5. Acknowledgements

This work was supported jointly by Key Project of National Natural Science Foundation of China (NSFC) under Grant No. 51636008, Key Research Program of Frontier Sciences, Chinese Academy of Science (CAS) under Grant No. QYZDB-SSW-JSC029, Fundamental Research Funds for the Central Universities under Grant No. WK2320000038 and Open Fund of State Key Laboratory of Fire Science (HZ2019-KF02).

6. References

[1] A.C. Fernandez-Pello, S.R. Ray, I. Glassman, Downward Flame Spread In an Opposed Forced Flow, Combustion Science and Technology, 2007;19: 19-30. https://doi.org/10.1080/00102207808946860

[2] I. Wichman, Flame spread in an opposed flow with a linear velocity gradient, Combustion and Flame, 1983;50: 287-304. https://doi.org/10.1016/0010-2180(83)90071-8

[3] I.S. Wichman, Theory of opposed-flow flame spread, Progress in Energy and Combustion Science, 1992;18: 553-93. https://doi.org/10.1016/0360-1285(92)90039-4

[4] J. De Ris. Spread of a laminar diffusion flame. Elsevier, 1969, pp. 241-52.

[5] L.-y. Zhao, J. Fang, X.-z. He, J.-w. Wang, S.-q. Tao, Y.-m. Zhang, An analysis of width effects on flame spread in conjunction with concurrent forced flow using a variable B-number, Combustion and Flame, 2018;194: 334-42. https://doi.org/10.1016/j.combustflame.2018.05.013

[6] F. Zhu, Z. Lu, S. Wang, Flame Spread and Extinction Over a Thick Solid Fuel in Low-Velocity Opposed and Concurrent Flows, Microgravity Science and Technology, 2015;28: 87-94.

[7] A.V. Singh, M.J. Gollner, Steady and transient pyrolysis of a non-charring solid fuel under forced flow, Proceedings of the Combustion Institute, 2017;36: 3157-65. https://doi.org/10.1016/j.proci.2016.07.043

[8] A.V. Singh, M.J. Gollner, Local Burning Rates and Heat Flux for Forced Flow Boundary-Layer Diffusion Flames, AIAA Journal, 2016;54: 408-18. https://doi.org/10.2514/1.J054283

[9] Y. Lu, X. Huang, L. Hu, C. Fernandez-Pello, The interaction between fuel inclination and horizontal wind: Experimental study using thin wire, Proceedings of the Combustion Institute, 2018.

[10] H.-T. Loh, A. Fernandez-Pello. A study of the controlling mechanisms of flow assisted flame spread. Elsevier, 1985, pp. 1575-82. https://doi.org/10.1016/S0082-0784(85)80652-4
[11] A. Kumar, A comparison of extinction limits and spreading rates in opposed and concurrent spreading flames over thin solids, Combustion and Flame, 2003;132: 667-77.
[12] M.J. Gollner, C.H. Miller, W. Tang, A.V. Singh, The effect of flow and geometry on concurrent flame spread, Fire Safety Journal, 2017;91: 68-78. https://doi.org/10.1016/j.firesaf.2017.05.007
[13] Y.H. C Chao, A.C. Fernandez-Pello, Concurrent Horizontal Flame Spread: The Combined Effect of Oxidizer Flow Velocity, Turbulence and Oxygen Concentration, Combustion Science and Technology, 1995;110-111: 19-51. https://doi.org/10.1080/00102209508951915
[14] L. Hu, A review of physics and correlations of pool fire behaviour in wind and future challenges, Fire safety journal, 2017;91: 41-55. https://doi.org/10.1016/j.firesaf.2017.05.008
[15] L. Hu, J. Hu, S. Liu, W. Tang, X. Zhang, Evolution of heat feedback in medium pool fires with cross air flow and scaling of mass burning flux by a stagnant layer theory solution, Proceedings of the Combustion Institute, 2015;35: 2511-2518. https://doi.org/10.1016/j.proci.2014.06.074
[16] L. Hu, S. Liu, L. Wu, Flame radiation feedback to fuel surface in medium ethanol and heptane pool fires with cross air flow, Combustion and Flame, 2013;160: 295-306.
[17] L. Hu, S. Liu, J. L. de Ris, A new mathematical quantification of wind-blown flame tilt angle of hydrocarbon pool fires with a new global correlation model, Fuel, 2013;106: 730-736.
[18] L. Hu, C. Kuang, X. Zhong, F. Ren, X. Zhang, H. Ding, An experimental study on burning rate and flame tilt of optical-thin heptane pool fires in cross flows, Proceedings of the Combustion Institute, 2017;36: 3089-3096. https://doi.org/10.1016/j.proci.2016.08.021
[19] J. Quintiere, The application of flame spread theory to predict material performance, Journal of Research of the National Bureau of Standards, 1988;93: 61-70.
[20] W. Tang, C.H. Miller, M.J. Gollner, Local flame attachment and heat fluxes in wind-driven line fires, Proceedings of the Combustion Institute, 2017;36: 3253-61. https://doi.org/10.1016/j.proci.2016.06.064
[21] X. Ju, M.J. Gollner, Y. Wang, W. Tang, K. Zhao, X. Ren, L. Yang, Downstream radiative and convective heating from methane and propane fires with cross wind, Combustion and Flame, 2019;204: 1-12. https://doi.org/10.1016/j.combustflame.2019.03.001
[22] L. Jiang, C.H. Miller, M.J. Gollner, J.-H. Sun, Sample width and thickness effects on horizontal flame spread over a thin PMMA surface, Proceedings of the Combustion Institute, 2017;36: 2987-94.
[23] X. Zhao, Y.-T.T. Liao, M.C. Johnston, S. James, P.V. Ferkul, S.L. Olson, Concurrent flame growth, spread, and quenching over composite fabric samples in low speed purely forced flow in microgravity, Proceedings of the Combustion Institute, 2017;36: 2971-78. https://doi.org/10.1016/j.proci.2016.06.028
[24] Y.-T. Tseng, S. James, Limiting length, steady spread, and nongrowing flames in concurrent flow over solids, Journal of heat transfer, 2010;132: 091201. https://doi.org/10.1115/1.4001645
[25] V. Apte, R. Bilger, A. Green, J. Quintiere, Wind-aided turbulent flame spread and burning over large-scale horizontal PMMA surfaces, Combustion and Flame, 1991;85: 169-84.
[26] M.J. Gollner, X. Huang, J. Cobian, A.S. Rangwala, F.A. Williams, Experimental study of upward flame spread of an inclined fuel surface, Proceedings of the Combustion Institute, 2013;34: 2531-38. https://doi.org/10.1016/j.proci.2012.06.063
[27] X. Huang, M. Gollner, Correlations for Evaluation of Flame Spread over an Inclined Fuel Surface, Fire Safety Science, 2014;11: 222-33. 10.3801/IAFSS.FSS.11-222
[28] X. Huang, S. Link, A. Rodriguez, M. Thomsen, S. Olson, P. Ferkul, C. Fernandez-Pello, Transition from opposed flame spread to fuel regression and blow off: Effect of flow, atmosphere, and microgravity, Proceedings of the Combustion Institute, 2018;37: 4117-4126. https://doi.org/10.1016/j.proci.2018.06.022